J Nanopart Res (2013) 15:1388
DOI 10.1007/s11051-012-1388-1

RESEARCH PAPER

Strong quantum confinement effects in SnS nanocrystals produced by ultrasound-assisted method

Yashar Azizian-Kalandaragh · Ali Khodayari · Zaiping Zeng · Christos S. Garoufalis · Sotirios Baskoutas · Lionel Cervera Gontard

Received: 3 June 2012 / Accepted: 21 December 2012

Abstract Nanocrystalline SnS powder has been prepared using tin chloride ($SnCl_2$) as a tin ion source and sodium sulfide (Na_2S) as a sulfur ion source with the help of ultrasound irradiation at room temperature. The as-synthesized SnS nanoparticles were quantitatively analyzed and characterized in terms of their morphological, structural, and optical properties. The detailed structural and optical properties confirmed the orthorhombic SnS structure and a strongly blue shifted direct band gap (1.74 eV), for synthesized nanoparticles. The measured band gap energy of SnS nanoparticles is in a fairly good agreement with the results of theoretical calculations of exciton energy based on the potential morphing method in the Hartree–Fock approximation.

Keywords Quantum confinement effect · SnS · Semiconductor nanoparticles · X-ray diffraction · Potential morphing method · Ultrasound irradiation

Y. Azizian-Kalandaragh (✉)
Department of Physics, University of Mohaghegh Ardabili, P.O. Box 179, Ardabil, Iran
e-mail: yashar.a.k@gmail.com; azizian@uma.ac.ir

A. Khodayari
Department of Chemistry, University of Mohaghegh Ardabili, P.O. Box 179, Ardabil, Iran

Z. Zeng · C. S. Garoufalis · S. Baskoutas
Materials Science Department, University of Patras, 26504 Patras, Greece

C. S. Garoufalis
Department of Environment Technology and Ecology, Technological Institute of Ionian Islands, 2 Kalvou Sq, 29100 Zakynthos, Greece

L. C. Gontard
Instituto de Ciencia de Materiales de Sevilla (CSIC), 41092 Sevilla, Spain

Introduction

Quantum confinement effect in semiconductor nanomaterials has been of special interest during the last decades. Quantum confined semiconductor nanocrystals, which exhibit properties different from bulk materials, are a new class of materials that hold considerable attention for numerous applications in the field of optoelectronics. Modification of molecular design and morphology of such nanostructures provides a powerful approach to control their electronic and optical properties. Reduction in the size of particles to nanometer ranges changes the degree of confinement of charge carriers, which affect the electronic and optical properties of semiconductor materials (Alivisatos 1996; Henglein 1989; Liu et al. 2006; Ögüt et al. 1997; Rama Krishna and Friesner 1991; Trindade et al. 2001). These unique characteristics of semiconductor nanostructured materials originate from the quantum confinement effects. From

Published online: 05 January 2013

theoretical point of view, as the radius of particle approaches the exciton Bohr radius of a given material, quantization of the energy bands become apparent and a blue shift in the exciton transition energy can be observed (Baskoutas and Terzis 2006; Wang and Herron 1990). Among the extensively studied IV–VI semiconductor materials, tin sulfide is very important narrow gap material because of its low toxicity and wide applications as an absorber layer in solar cells, near infrared materials, holographic recording media, and solar control devices (Liu et al. 2010; Rudel 2003; Winship 1998). It is important and necessary to study the band gap changes in semiconductor nanostructures in order to gain a better understanding for their relevant properties. Also, band gap engineering of the semiconductor nanostructures by the control of nanostructure sizes is important. Experimental studies showed that semiconductor SnS exhibit p and n type conduction and has both a direct optical gap located at 1.3 eV and indirect optical band gap located at 1.1 eV (Bashkirov et al. 2011; Ning et al. 2010; Yue et al. 2009). In order to obtain nanostructured SnS, the following methods are used: spray pyrolysis of the water solution (Reddy et al. 1999; Thangaraju and Kaliannan 2000), vacuum evaporation (Johson et al. 1999), chemical vapor deposition (Ortiz et al. 1996; Price et al. 2000), chemical bath deposition (Engelken et al. 1987; Tanusevski 2003), electro deposition and electrochemical deposition (Chazali et al. 1998; Takeuchi et al. 2003), chemical synthesis (Gou et al. 2005), microwave assisted synthesis (Chen et al. 2004), mild solution route (Li et al. 2002), modified solution dispersion method (Zhao et al. 2004), two gas process (Reddy and Reddy 2002), solvothermal process (Panda et al. 2006; Paul and Agarwal 2007; Paul et al. 2008; Qian et al. 1999), successive ionic layer adsorption and reaction (SILAR) method (Ghosh et al. 2008), hydrothermal synthesis (Biswas et al. 2007), and molecular beam epitaxy (Nozaki et al. 2005).

Generally, most of the above-mentioned methods require high temperature as well as the use of highly sensitive toxic solvents. Our attempt is to obtain high quality materials under normal laboratory conditions, using safer precursors by applying ultrasonic waves. Previously ultrasonic waves have been used for the preparation of nanomaterials (Azizian-Kalandaragh et al. 2009; Azizian-Kalandaragh and Khodayari 2010a, b; Bhattacharyya and Gedanken 2008; Goharshadi et al. 2009; Suslick 1990; Suslick et al. 1990; Wang et al. 2002; Zhu et al. 2008).

Ultrasonic waves have been shown to cause physical and chemical effects such as fragmentation to small particles and acceleration of reactions, which may be used for the preparation of new materials with desirable properties.

During sonication, ultrasonic longitudinal waves are radiated through the solution causing alternating high and low pressure regions in the liquid medium. Millions of microscopic bubbles form and grow in the low-pressure stage, and subsequently collapse in the high-pressure stage.

Hot spots that are localized regions of extremely high temperatures as high as 5,000 K, and pressures of up to $\sim$1,800 atm can occur from the collapsing bubbles, and cooling rates can often exceed $\sim 10^{10}$ K s^{-1}. The energy released from this process, known as cavitation, would lead to enhanced chemical reactivity and accelerated reaction rates (Suslick 1988).

In this paper we report the preparation of SnS nanocrystals with the help of ultrasonic irradiation. We have chosen this method because of its many advantages, such as easier composition control, low toxicity, better homogeneity, low processing temperature, easier fabrication of large numbers of nanoparticles, lower cost, and possibility of using high purity starting materials. In this paper we also report the morphological, optical, and structural properties of SnS nanocrystals. As our results indicate, the absorption edge is shifted toward the lower wavelength side (i.e., blue shift) and direct energy gap of SnS nanocrystals is estimated to 1.74 eV. The results are compared to theoretical calculations based on the potential morphing method (PMM) (Rieth et al. 2002) in the Hartree–Fock approximation (Baskoutas 2005a, b; Baskoutas et al. 2006a, b; Baskoutas and Terzis 2006; Poulopoulos et al. 2011). This method, based on the adiabatic theorem of quantum mechanics which states that if the Hamiltonian of the system varies slowly with time then the nth eigenstate of the initial Hamiltonian will be carried into the nth eigenstate of the final Hamiltonian, solves the Schrödinger equation for any arbitrary interaction potential. In the present case, the PMM based results exhibit a fairly good agreement with the experimental data. This combined experimental and theoretical work provides a better insight on the quantum confinement effects in SnS nanoscaled systems.

Experimental details

Materials and instruments

Sodium sulfide hydrate was obtained from Sigma-Aldrich, triethanolamine (TEA) was obtained from Rankem; tin (II) chloride dihydrate, polyvinyl alcohol (PVA), and absolute ethanol were obtained from Merck. All the reagents were used as-received without purification.

X-ray diffraction (XRD) analysis of drop-coated films on an ordinary glass substrate from the SnS nanocrystals was carried out on a Philips X' Pert Pro with CuKα radiation. The optical properties of sample were monitored on a Carry 5 UV-Visible spectrophotometer (model Varian). Scanning electron microscopy (SEM) measurements were performed on a LEO 1430VP instrument operated at an accelerating voltage of 15 kV. The elemental analyses of the products were obtained by energy dispersive X-ray analysis (EDAX) on the same LEO 1430VP instrument with accelerating voltage of 15 kV. Samples for SEM and EDAX studies were prepared by placing drops of the SnS nanostructured suspension on gold- and palladium-coated SEM stage. Transmission electron microscopy (TEM) images of the sample were taken on a Philips CN10, TEM performing at an accelerating voltage of 100 kV.

Preparation of SnS nanocrystals

In a typical procedure, for preparation of 0.2 M solution of tin chloride, 0.90 g of tin chloride powder was dissolved in 20 ml TEA, then 0.31 g of sodium sulfide was dissolved in 20 ml distilled water (0.2 M). These two solutions were mixed and were put in a 100 ml round bottom flask. The pH value of the mixture was 12. The mixture solutions were kept under high intensity ultrasonic transductor at room temperature for 2 h. During irradiation 5 ml of aqueous solutions of PVA (1 %) were added to the mixture. At the end of the reaction, a great amount of black precipitates were obtained. After cooled to room temperature, the precipitates were centrifuged, washed by distilled water and absolute ethanol in sequence, and dried in vacuum. Plenty of SnS nanoparticles have been prepared using this method and the yield of this preparation is high in comparison with most of chemical preparation methods. The final products were collected for characterizations. The products were characterized by XRD, SEM, TEM, EDAX, and UV-Visible spectroscopy.

The formation mechanism of SnS nanocrystals with the reaction equation can be expressed as follows:

$$SnCl_2 \cdot 2H_2O + Na_2S \cdot \ xH_2O \rightarrow SnS + 2NaCl + xH_2O$$

The role of PVA is to stabilize the nanostructures preventing them from coagulation.

Theory

In the effective mass approximation the Hamiltonian for the electron hole system can be written as (Baskoutas 2005a, b; Baskoutas et al. 2006a, b; Baskoutas and Terzis 2006; Poulopoulos et al. 2011)

$$H = -\frac{\hbar^2}{2m_e^*}\nabla_e^2 - \frac{\hbar^2}{2m_h^*}\nabla_h^2 + V_0^e(r_e) + V_0^h(r_h) - \frac{e^2}{\varepsilon}\frac{1}{r_{eh}} \quad (1)$$

where m_e^* (m_h^*) is the effective electron (hole) band mass, ε is the effective dielectric constant, r_{eh} is the electron—hole distance in three dimensions, and $V_0^{e(h)}$ is the finite depth well confinement potential of electron (hole). As in our previous work (Poulopoulos et al. 2011; Baskoutas et al. 2006a, b) we will also use here a reliable expression for the dielectric constant ε developed by Hanken (1956) and used by several authors for example Nanda et al. (2004); Pellegrini et al. (2005) and which has the following form

$$\frac{1}{\varepsilon(R_0)} = \frac{1}{\varepsilon_\infty} - \left[\frac{1}{\varepsilon_\infty} - \frac{1}{\varepsilon_0}\right]\left[1 - \frac{\exp\left(-R_0/\rho_e\right) + \exp\left(-R_0/\rho_h\right)}{2}\right] \quad (2)$$

where R_0 is the mean distance between the electron and hole (Nanda et al. 2004; Pellegrini et al. 2005) and approximately takes the values (Nanda et al. 2004) $0.69932R$ or R (Baskoutas et al. 2006a, b), where R is the radius of the cluster and represents half of the confining parameter which is the diameter of the

nanocrystal. ε_0 and ε_∞ are the static and optical dielectric constants, respectively, and $\rho_{e,h}$ are given as follows

$$\rho_{e,h} = \left(\frac{\hbar}{2m^*_{e,h}\omega_{LO}}\right)^{1/2} \tag{3}$$

where ω_{LO} is the frequency of LO phonons.

As regards the height of the finite depth well confining potentials $V_0^{e(h)}$ for electrons and holes, we have shown in our previous study (Baskoutas and Terzis 2006) that is independent of the nanostructured semiconductor material and depends exclusively on the matrix energy band gap $E_g(M)$ by a simple linear relation of the form $V_0 = 0.08 \cdot E_g(M)$. Assuming also that the confining potential has the same value for both electron and hole, we set for our thin film system

$$V_0^e(r_e) = V_0^h(r_h) = \begin{cases} 0 & r < R \\ 0.08 \cdot E_g(M) & r \geq R \end{cases} \tag{4}$$

where R is the radius of the nanocrystal.

The Hartree–Fock equations are solved in an iterative manner until self consistency is achieved. In each iteration the PMM (Baskoutas 2005a, b; Baskoutas et al. 2006a, b; Baskoutas and Terzis 2006; Poulopoulos et al. 2011) is employed as a subroutine for the calculation of the corresponding energies and wavefunctions and thus the Hartree–Fock potential for the next iteration. Actually, PMM solves the time-independent Schrödinger equation for an arbitrary interaction potential $v_S(\vec{r})$ starting from a potential $v_R(\vec{r})$ with well-known eigenvalues and eigenfunctions. The essential point is that the transition from potential $v_R(\vec{r})$ to the potential $v_S(\vec{r})$ by means of the time-dependent Schrödinger equations as follows: using the potential $v_R(\vec{r})$ and $v_S(\vec{r})$, we formulate a time-dependent Schrödinger equation (Rieth et al. 2002)

$$i\hbar\frac{\partial\Phi(\vec{r},t)}{\partial t} = \left\{-\frac{\hbar^2}{2m}\nabla^2 + (1-\sigma(t))v_R(\vec{r}) + \sigma(t)v_s(\vec{r})\right\}\Phi(\vec{r},t), \tag{5}$$

where σ(t) has the following property:

$$\sigma(t) = \begin{cases} 0, & t \leq t_a \\ 1, & t \geq t_b \end{cases}. \tag{6}$$

For $t_a \leq t \leq t_b$ ($t_a$is the morphing starting moment, $t_b$is the morphing ending moment). The function $\sigma(t)$ should increase monotonically. Moreover, we solve equation (5) numerically. After a large number of time steps (so that $t > t_b$), the energy eigenvalue E_S for the potential $v_S(\vec{r})$ is given by

$$E_S = \int d^3r\Phi_S^*(\vec{r})\left\{-\frac{\hbar^2}{2m}\nabla^2 + v_S(\vec{r})\right\}\Phi_S(\vec{r}), \tag{7}$$

where Φ_S is the wave function of the system under consideration. In the present calculations, the reference system for PMM is set to be the three-dimensional harmonic oscillator with the well-known eigenfunctions (Greiner 1989)

$$\Phi_{nlm}(r,\theta,\varphi) = r^l e^{-\frac{m\omega}{2\hbar}r^2}{}_1F_1\left(-n, l+3/2, \lambda r^2\right)Y_{lm}(\theta,\varphi) \tag{8}$$

where ${}_1F_1(-n, l+3/2, \lambda r^2)$ is the hypergeometric function (Greiner 1989). The interaction potential is

$$v_S(\vec{r}) = v_{HF}(\vec{r}) + v_C(\vec{r}), \tag{9}$$

where $v_{HF}(\vec{r})$ is the Hartree–Fock potential for the electron (or hole), while $v_C(\vec{r})$ is the electron (or hole) confinement potential which is given explicitly in Eq. (4). It should be noted here that adopting the harmonic oscillator as a reference system does not affect our results because the PMM needs only a known reference system to start the morphing process and finally to give the eigenfunctions and eigenvalues for the unknown system, independently from the choice of the initial reference system (Rieth et al. 2002).

When the procedure reaches a self consistent solution, then the exciton energy is calculated by the sum of the corresponding electron and hole energies

$$E(X) = \tilde{E}_e + \tilde{E}_h \tag{10}$$

and the effective band gap is given by (Baskoutas 2005a, b; Baskoutas et al. 2006a, b; Baskoutas and Terzis 2006; Poulopoulos et al. 2011)

$$E_B = E_g + E(X) \tag{11}$$

where E_g is the bulk band gap energy.

Results and discussion

The quantitative analysis of the as-prepared product was carried out using the EDAX technique. Figure 1 shows typical EDAX spectrum and details of relative analysis for SnS nanocrystals. The spectrum illustrates

the actual distribution of Sn and S of the prepared sample separately. It is evident from the analysis that the product contains Sn and S materials with a same average atomic percentage ratio (1:1). Note that non-labeled peaks in EDAX spectrum comes from the Au–Pd sputter coating and glass stage.

The morphology of the as-prepared products was studied by SEM. The SEM image (Fig. 2) show that the product consists of very small spherical SnS nanocrystallites aggregated in the form of polydispersive nanoclusters with sizes smaller than 100 nm. It is very hard to discuss about nanoparticles size using SEM images, but from images it is clear that the sizes are in the order of very small nanoparticles.

In order to further elucidate the morphology and the size of nanoparticles, TEM image was taken and is shown in Fig. 3. Comparison of TEM and SEM images confirms the formation of very small spherical SnS nanoparticles, most of which aggregated together in the form of polydispersive nanoclusters.

The particle size distribution was also measured from the bright-field TEM image shown in Fig. 4. The detection and measurement of the nanoparticles (segmentation) on this type of samples is difficult because thickness changes locally, and diffraction from different crystal orientations introduce large contrast variations. First, the image was preprocessed by adjusting the contrast and brightness to minimize the speckle contrast of the background due to the carbon film used to support the sample. Second, the SnS

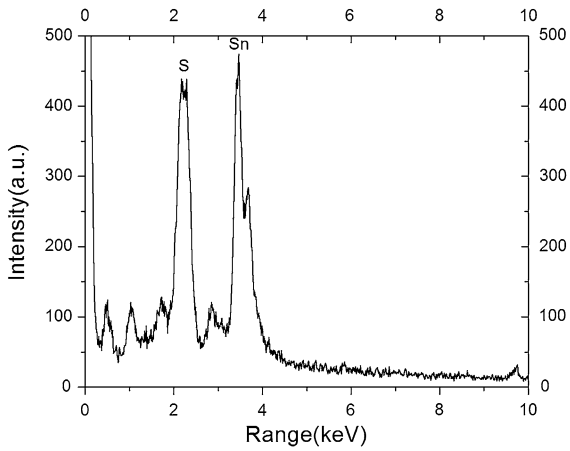

Fig. 1 EDAX spectrum of the as-prepared SnS nanocrystals

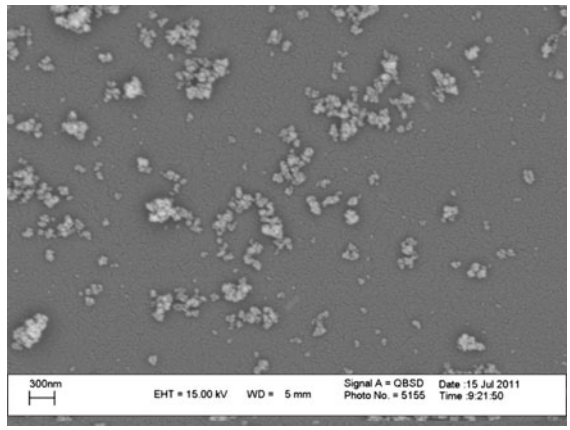

Fig. 2 SEM image of the as-prepared SnS nanocrystals

nanoparticles were segmented using a semiautomatic procedure which combines interactive segmentation with adaptative thresholding, obtaining an mean particle diameter of 3.2 nm with a standard deviation of 1.9 nm (Gontard et al. 2011).

Figure 5 show the XRD pattern of the as-prepared SnS nanocrystals. Several peaks corresponding to diffraction of orthorhombic SnS appear clearly in the

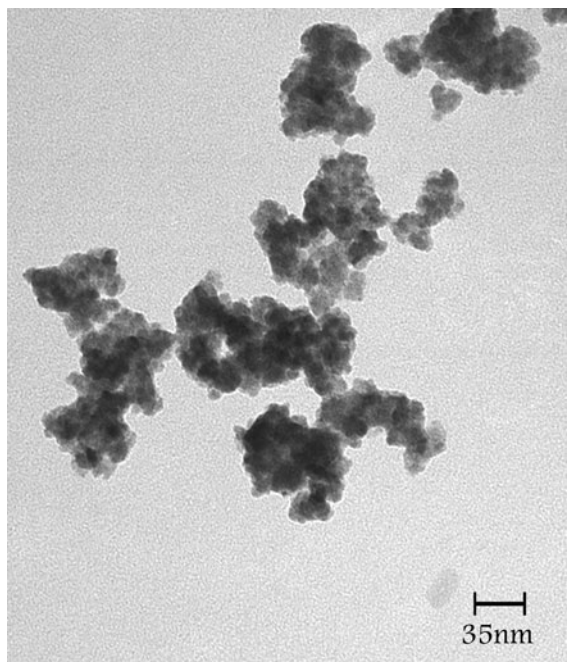

Fig. 3 Typical TEM image of SnS nanocrystals

figure. This clearly proves polycrystalline nature of the as-prepared product in which the appeared peaks are very consistent with the values in the standard card of SnS phase (JCPDS No. 39-0354).The broadness of the peaks indicates that the size of structure is reasonably nanocrystalline in nature. The crystallite size of SnS nanoparticles was calculated using Debye–Scherrer formula (Guinier 1963) $D = \frac{0.9\lambda}{\beta\cos(\theta)}$. Here, D is the coherent length, λ the wave length of X-ray radiation, β the full-width at half-maxima (FWHM) of the prominent peak, and θ is the angle of diffraction. So the corresponding crystallite size of nanoparticles obtained are smaller than 4 nm in the case of broadened peaks.

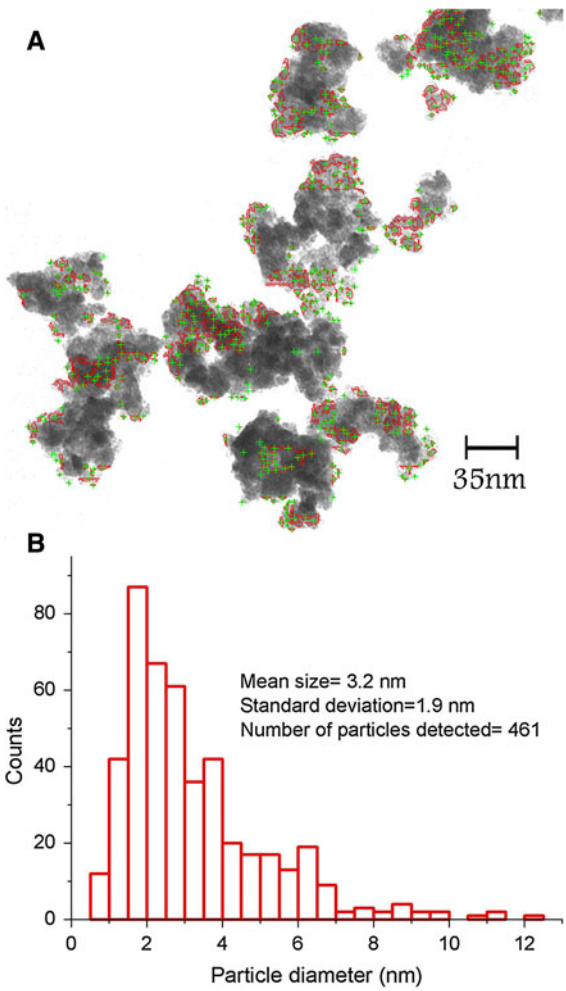

Fig. 4 **a** Image on which an over layer of the boundaries and center of masses of the segmented particles has been added to the original bright-field TEM image shown in Fig. 3. Adaptative thresholding with 80 × 80 divisions and a kernel size of 5 pixels was used. **b** Histogram of the size distribution of the nanoparticles and several statistical parameters

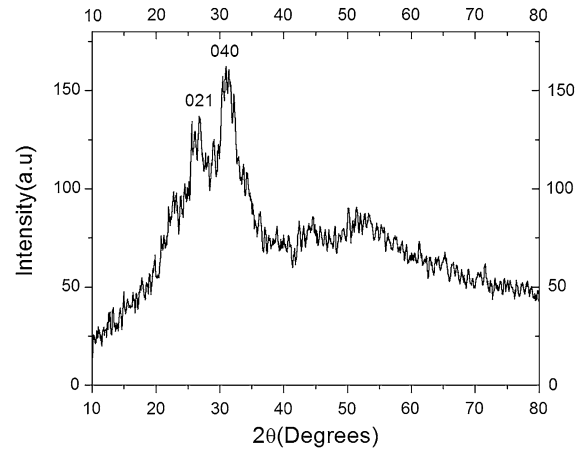

Fig. 5 XRD pattern of the as-prepared SnS nanocrystals

Figure 6 shows the plot of $(\alpha hv)^2$ versus photon energy (hv) of the SnS nanocrystals and also absorption spectrum of the as-prepared SnS nanocrystals. Investigations prove that the absorption reduces rapidly with the increase of wavelength. These values were used to determine absorption coefficientα. The absorption coefficient α of SnS nanocrystals was calculated from the average absorption index A as $\alpha = \frac{4\pi A}{\lambda}$ (Suslick 1988). The optical energy gap of the SnS nanocrystal was evaluated using the relation $\alpha = \frac{A\left(hv - E_g\right)^n}{hv}$ where A is an energy independent constant and n characterizes the transition process (El-Nahass et al. 2002).

The curve has a good straight line fit with higher energy range above the absorption edge, indicating a direct optical transition edge. Based on Fig. 6, the direct energy gap of the sample has been calculated as 1.74 eV which is blue shifted in comparison to the bulk band gap.

Now in order to investigate the above system theoretically with PMM we assume that the matrix is PVA with $E_g(M) = 4.98$ eV (Mahendia et al. 2011) and we use the following material parameters for SnS: $m_e^* = 0.5\ m_0$ (Vidal et al. 2012), $m_h^* = 0.109\ m_0$ (Reddy and Reddy 2006), where m_0 is the electron mass, $\varepsilon_0 = 32$ (Chandrasekhar et al. 1977) and $\varepsilon_\infty = 16$ (Chandrasekhar et al. 1977) and $\hbar\omega_{LO} = 71$ meV (Chandrasekhar et al. 1977) and$E_g(\text{bulk}) = 1.296$ eV

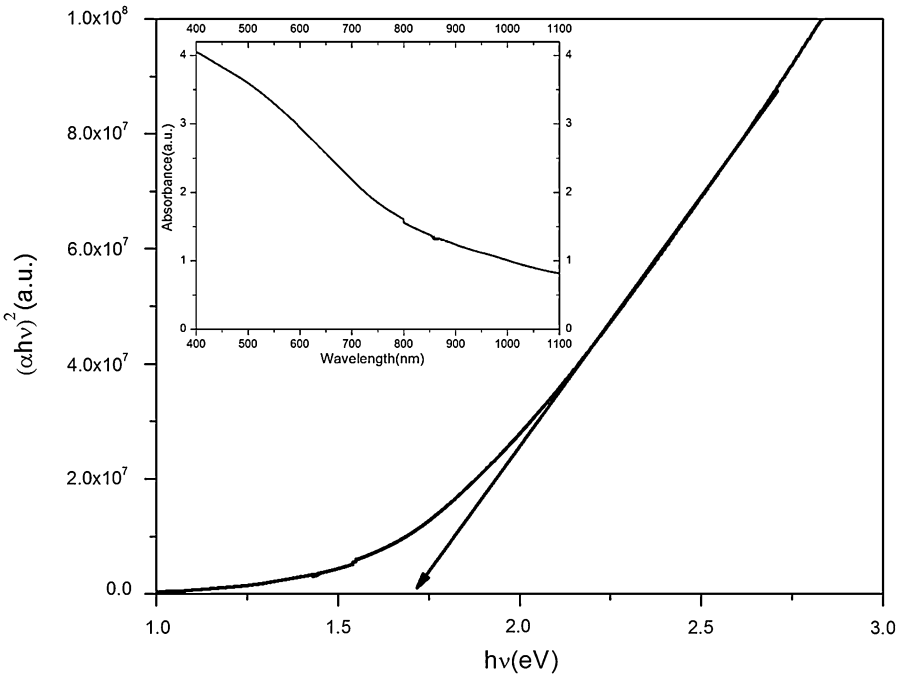

Fig. 6 Plot of $(\alpha h\nu)^2$ versus and Uv–Visible absorption spectrum of the as-prepared SnS nanocrystals

(Parenteau and Carlone, 1990). The effective band gap is calculated according to the relation (11) and the theoretical results are depicted in Fig. 7. The size of the nanocrystals which can be estimated from the curve of Fig. 7 is 4 nm (corresponding to the energy value 1.74 eV) and is in a fairly good agreement with the size which is obtained from the Debye–Scherrer formula and TEM image analysis.

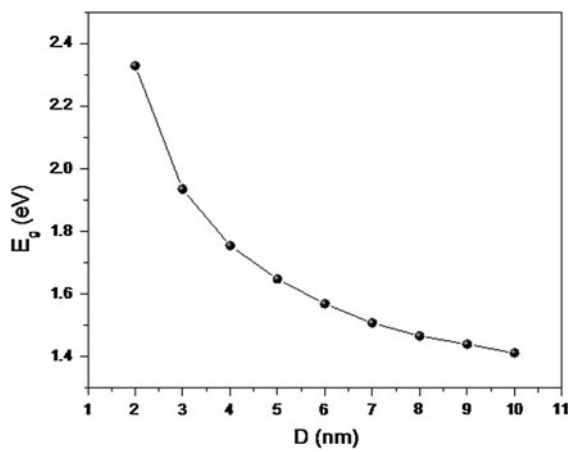

Fig. 7 Theoretical curve of the optical band gap as a function of the nanocrystal radius (with PMM in the Hartree–Fock approximation)

Conclusion

In conclusion, for the first time, using a novel, very simple and not expensive procedure, SnS nanocrystals have been synthesized via ultrasonic waves at normal laboratory conditions. The as-synthesized SnS nanocrystals were quantitatively analyzed and characterized in terms of their morphological, structural, and optical properties. The SnS nanocrystals appear strongly blue shifted with direct band gap energy value of 1.74 eV. Comparison with the theoretical curve of the exciton energy versus the particle size, which is obtained with the PMM method in the Hartree–Fock approximation, shows a fairly good agreement indicating that the observed blue shift is attributed clearly to the effect of the quantum confinement.

Acknowledgments The support by the University of Mohaghegh Ardabili, Ardabil, Iran, to carry out this study is gratefully acknowledged. The authors (S. Baskoutas, Z. Zeng and Ch. S. Garoufalis) acknowledge the European Union (European Regional Development Fund-ERDF) and Greek national funds through the Operational Program "Regional Operational Programme" of the National Strategic Reference

Framework (NSRF)-Research Funding Program: Support for research, technology and innovation actions in Region of Western Greece (MIS: 312123, D.237.002) for financial supports.

References

Alivisatos AP (1996) Perspectives on the physical chemistry of semiconductor nanocrystals. J Phys Chem 100:13226–13239

Azizian-Kalandaragh Y, Khodayari A (2010a) Ultrasound-assisted preparation of CdSe nanocrystals in the presence of Polyvinyl alcohol as a capping agent. Mater Sci Semicond Process 13:225–230

Azizian-Kalandaragh Y, Khodayari A (2010b) Aqueous synthesis and characterization of nearly monodispersed ZnS nanocrystals. Phys Status Solidi A 207(9):2144–2148

Azizian-Kalandaragh Y, Khodayari A, Behboudnia M (2009) Ultrasound-assisted synthesis of ZnO semiconductor nanostructures. Mater Sci Semicond Process 12:142–145

Bashkirov SA, Gremenok VF, Ivanov VA (2011) Physical properties of SnS thin films fabricated by hot wall deposition. Fizika i Tekhnika Poluprovodnikov 45:765–769

Baskoutas S (2005a) Excitons and charged excitons in InAs nanorods. Chem Phys Lett 404:107–111

Baskoutas S (2005b) Novel formulation of the Hartree–Fock approximation: effective band gap calculation of InAs nanorods. Phys Lett A 341:303–307

Baskoutas S, Terzis AF (2006) Size-dependent band gap of colloidal quantum dots. J Appl Phys 99:013708

Baskoutas S, Poulopoulos P, Karoutsos V, Angelakeris M, Flevaris NK (2006a) Strong quantum confinement effects in thin zinc selenide films. Chem Phys Lett 417:461–464

Baskoutas S, Terzis AF, Schommers W (2006b) Size-Dependent exciton energy of narrow band gap colloidal quantum dots in the finite depth square-well effective mass approximation. J Comp Theor Nanosci 3:269–271

Bhattacharyya S, Gedanken A (2008) A template-free, sonochemical route to porous ZnO nano-disks. Microporous Mesoporous Mater 110:553–559

Biswas S, Kar S, Chaudhuri S (2007) Thioglycolic acid (TGA) assisted hydrothermal synthesis of SnS nanorods and nanosheets. Appl Surf Sci 253:9259–9266

Chandrasekhar HR, Humphreys RG, Zwick U, Cardona M (1977) Infrared and Raman spectra of the IV-VI compounds SnS and SnSe. Phys Rev B 15:2177–2183

Chazali A, Zainal Z, Hussein MZ, Kassim A (1998) Cathodic electrodeposition of SnS in the presence of EDTA in aqueous media. Sol Energy Mater Sol Cells 55:237–249

Chen D, Shen G, Tang K, Lei S, Zheng H, Qian Y (2004) Microwave-assisted polyol synthesis of nanoscale SnS_x ($x = 1, 2$) flakes. J Cryst Growth 260:469–474

El-Nahass MM, Zeyada HM, Aziz MS, El-Ghamaz NA (2002) Optical properties of thermally evaporated SnS thin films. Opt Mater 20:159–170

Engelken RD, McCloud HE, Lee C, Slayton M, Ghoreishi H (1987) Low temperature chemical precipitation and vapor deposition of Sn_x S thin films. J Electrochem Soc 134:2696–2707

Ghosh B, Das M, Banerjee P, Das S (2008) Fabrication and optical properties of SnS thin films by SILAR method. Appl Surf Sci 254:6436–6440

Goharshadi EK, Ding Y, Jorabchi MN, Nancarrow P (2009) Ultrasound-assisted green synthesis of nanocrystalline ZnO in the ionic liquid [hmim][NTf_2]. Ultraso Sonochem 16:120–123

Gontard LC, Ozkaya D, Dunin-Borkowski R (2011) A simple algorithm for measuring particle size distributions on an uneven background from TEM images. Ultramicroscopy 111:101–106

Gou XL, Chen J, Shen PW (2005) Synthesis, characterization and application of SnS_x ($x = 1, 2$) nanoparticles. Mater Chem Phys 93:557–566

Greiner W (1989) Quantum mechanics: an introduction. Springer, Berlin

Guinier A (1963) X-Ray diffraction. In: Crystals, imperfect crystals, and amorphous bodies, Freeman, Sanfrancisco

Hanken H (1956) Nuovo Cim 3:1230

Henglein A (1989) Small-particle research: physicochemical properties of extremely small colloidal metal and semiconductor particles. Chem Rev 89:1861–1873

Johson JB, Jones H, Latham BS, Parker JD, Engelken RD, Barber C (1999) Optimization of photoconductivity in vacuum-evaporated tin sulfide thin films. Semicond Sci Technol 14:501–507

Li Q, Ding Y, Wu H, Liu X, Qian Y (2002) Fabrication of layered nanocrystallites SnS and β-SnS2 via a mild solution route. Mater Res Bull 37:925–932

Liu Y, Xu Y, Li JP, Zhang B, Wu D, Sun YH (2006) Synthesis of CdS_xSe_{1-x} nanorods via a solvothermal route. Mater Res Bull 41:99–109

Liu H, Liu Y, Wang Z, He P (2010) Facile synthesis of monodisperse, size-tunable SnS nanoparticles potentially for solar cell energy conversion. Nanotechnology 21:105707

Mahendia S, Tomar AK, Chahal RP, Goyal P, Kumar S (2011) Optical and structural properties of poly(vinyl alcohol) films embedded with citrate-stabilized gold nanoparticles. J. Phys. D 44:205105

Nanda KK, Kruis FE, Fissan H (2004) Effective mass approximation for two extreme semiconductors: band gap of PbS and CuBr nanoparticles. J Appl Phys 95:5035–5043

Ning J, Men K, Xiao G, Wang L, Dai Q, Zou B, Liu B, Zou G (2010) Facile synthesis of IV–VI SnS nanocrystals with shape and size control: nanoparticles, nanoflowers and amorphous nanosheets. Nanoscale 2:1699–1703

Nozaki H, Onoda M, Dekita M, Kosuda K, Wada T (2005) Variation of lattice dimensions in epitaxial SnS films on MgO(001). J Solid State Chem 178:245–252

Ögüt S, Chelikowsky JR, Louie SG (1997) Quantum confinement and optical gaps in Si nanocrystals. Phys Rev Lett 79:1770–1773

Ortiz A, Alonso JC, Garcia M, Toriz J (1996) Tin sulphide films deposited by plasma-enhanced chemical vapour deposition. Semicond Sci Technol 11:243–247

Panda SK, Gorai S, Chaudhuri S (2006) Shape selective solvothermal synthesis of SnS: role of ethylenediamine–water solvent system. Mater Sci Eng B 129:265–269

Parenteau M, Carlone C (1990) Influence of temperature and pressure on the electronic transitions in SnS and SnSe semiconductors. Phys Rev B 41:5227–5234

Paul GS, Agarwal P (2007). Structural and stability studies of SnS nanoflakes synthesized by solvothermal process for solar photovoltaic applications. IEEE Conference Proceedings, pp. 884–886

Paul GS, Gogoi P, Agarwal P (2008) Structural and stability studies of CdS and SnS nanostructures synthesized by various routes. J Non-Cryst Solids 354:2195–2199

Pellegrini G, Mattei G, Mazzoldi P (2005) Finite depth square well model: applicability and limitations. J Appl Phys 97:073706–073713

Poulopoulos P, Baskoutas S, Pappas SD, Garoufalis CS, Droulias SA, Zamani A, Kapaklis V (2011) Intense quantum confinement effects in Cu_2O thin films. J Phys Chem C 115:14839–14843

Price LS, Parkin IP, Field MN, Hardy AME, Clark RJH, Hibbert TG, Molloy KC (2000) Atmospheric pressure chemical vapour deposition of tin(II) sulfide films on glass substrates from $Bun_3SnO_2CCF_3$ with hydrogen sulfide. J Mater Chem 10:527–530

Qian XF, Zhang XM, Wang C, Wang WZ, Xie Y, Qian YT (1999) Solvent–thermal preparation of nanocrystalline tin chalcogenide. J Phys Chem Solids 60:415–417

Rama Krishna MV, Friesner RA (1991) Quantum confinement effects in semiconductor clusters. J Chem Phys 95:8309–8322

Reddy KTR, Reddy PP (2002) Structural studies on SnS films grown by a two-stage process. Mater Lett 56:108–111

Reddy NK, Reddy KTR (2006) Optical behaviour of sprayed tin sulphide thin films. Mat Res Bull 41:414–422

Reddy NK, Reddy KTR, Fisher G, Best R, Dutta PK (1999) The structural behaviour of layers of SnS grown by spray pyrolysis. J Phys D 32:988–990

Rieth M, Schommers W, Baskoutas S (2002) Exact numerical solution of Schrödinger's equation for a particle in an interaction potential of general shape. Int J Mod Phys B 16:4081

Rudel H (2003) Case study: bioavailability of tin and tin compounds. Ecotoxicol Environ Saf 56:180–189

Suslick KS (1988) Ultrasound: its chemical, physical, and biological effects. VCH, New York

Suslick KS (1990) Sonochemistry. Science 247:1439–1445

Suslick K, Doktycz S, Flint E (1990) On the origin of sonoluminescence and sonochemistry. Ultrasonics 28:280–290

Takeuchi K, Ichimura M, Arai E, Yamazaki Y (2003) SnS thin films fabricated by pulsed and normal electrochemical deposition. Sol Energy Mater Sol Cells 75:427–432

Tanusevski A (2003) Optical and photoelectric properties of SnS thin films prepared by chemical bath deposition. Semicond Sci Technol 18:501

Thangaraju B, Kaliannan P (2000) Spray pyrolytic deposition and characterization of SnS and SnS_2 thin films. J Phys D 33:1054–1059

Trindade T, O'Brien P, Pickett NL (2001) Nanocrystalline semiconductors: synthesis, properties, and perspectives. Chem Mater 13:3843–3858

Vidal J, Lany S, d'Avezac M, Zunger A, Zakutayev A, Francis J, Tate J (2012) Band-structure, optical properties, and defect physics of the photovoltaic semiconductor SnS. Appl Phys Lett 100:032104–032107

Wang Y, Herron N (1990) Quantum size effects on the exciton energy of CdS clusters. Phys Rev B 42:7253–7255

Wang H, Zhang JR, Zhao XN, Xu S, Zhu JJ (2002) Preparation of copper monosulfide and nickel monosulfide nanoparticles by sonochemical method. Mater Lett 55:253–258

Winship KA (1998) Toxicity of tin and its compounds. Adverse Drug React Acute Poisoning Rev 7:19–38

Yue GH, Peng DL, Yan PX, Wang LS, Wang W, Luo XH (2009) Structure and optical properties of SnS thin film prepared by pulse electrodeposition. J Alloy Compd 468:254–257

Zhao Y, Zhang Z, Dang H, Liu W (2004) Synthesis of tin sulfide nanoparticles by a modified solution dispersion method. Mater Sci Eng B 113:175–178

Zhu L, Meng J, Cao X (2008) Sonochemical synthesis of monodispersed KY_3F_{10}:eu^{3+} nanospheres with bimodal size distribution. Mater Lett 62:3007–3009